

<sup>8</sup>In this equation and the others which follow, an overall energy-momentum conservation  $\delta$  function between the initial and final states, present in each term, is implicitly understood.

<sup>9</sup>In the Bethe-Salpeter equation, we are off the mass

shell but on the energy-momentum shell.

<sup>10</sup>T. C. Chen and K. Raman, Phys. Rev. D **3**, 505 (1971).

<sup>11</sup>R. J. Yaes, Phys. Rev. **170** 1236, (1968); Nucl. Phys. **A131** 623, (1969).

PHYSICAL REVIEW D

VOLUME 3, NUMBER 12

15 JUNE 1971

## Numerical Studies of the Bethe-Salpeter Equation and the Multiperipheral Integral Equation of Amati, Bertocchi, Fubini, Stanghellini, and Tonin\*

H. W. Wyld, Jr.

*Physics Department, University of Illinois, Urbana, Illinois 61801*

(Received 25 January 1971)

We present some numerical results for Regge poles determined from the Bethe-Salpeter equation with scalar couplings. Both the trajectories and residue functions are determined. We find that it is a good approximation to ignore the coupling between different  $O(4)$  states. The effect of a second-order correction to the potential (the crossed-box graph) is studied and evaluated numerically. The relation of the Bethe-Salpeter equation with the multiperipheral integral equation is reviewed, and we show how to solve the latter equation by numerical iteration. Some results are given which do not exhibit any oscillations in the total cross section.

### I. INTRODUCTION

For twenty years the Bethe-Salpeter equation<sup>1,2</sup> has been of great interest in particle physics because it provides a relativistically covariant, yet tractable, equation for a two-body bound state or scattering state. In its simplest form (the ladder approximation) the equation sums the series of Feynman graphs illustrated in Fig. 1 and is thus formally similar to the nonrelativistic Schrödinger equation with a potential corresponding to a rung of the ladder. In 1962 a big advance was made by Lee and Sawyer,<sup>3</sup> who showed that the Bethe-Salpeter scattering amplitude in the ladder approximation with scalar couplings is meromorphic in the complex angular momentum half-plane  $\text{Re } l \geq -\frac{3}{2}$  with at least one Regge pole in this region. In simple terms the Regge poles are just bound states for arbitrary (nonintegral) values of  $l$ . More recently extensive use was made of the Bethe-Salpeter equation by Domokos and Suranyi<sup>4</sup> and by Freedman and Wang<sup>5</sup> in their study of daughter trajectories.

The important point, with respect to the daughter trajectories, is the four-dimensional rotational invariance of the equation as applied to a bound state with total energy zero [ $P=0$  in Eq. (1) below]. For nonzero values of the total energy the equation has the usual three-dimensional rotational invariance. At zero energy the additional symmetry implies that the Regge poles appear in families, a

leading trajectory at  $l = \alpha$  with daughters at  $l = \alpha - 1, \alpha - 2, \dots$ . This  $O(4)$  symmetry is also extremely important for the practical purpose of solving the equation numerically, and this is the point we are most interested in for this paper. Because of its covariant structure the Bethe-Salpeter equation is a four-dimensional integral equation. If one makes the usual angular momentum decomposition, one obtains a two-dimensional integral equation. While it may be feasible to solve such an equation numerically on a computer in simple cases, it is certainly difficult and expensive. On the other hand, for total energy zero the additional symmetry allows us to expand in four-dimensional spherical harmonics. The equations decouple and we are left with a one-dimensional integral equation. This can be easily solved numerically by approximating it by a matrix equation. At nonzero total energy the four-dimensional symmetry of the equation is broken. However, we can still expand in four-dimensional spherical harmonics to obtain coupled one-dimensional integral equations. If we are sufficiently close to zero total energy, the coupling between amplitudes will be small and we need keep only a few coupled amplitudes to obtain an accurate result. Some numerical calculations of the Regge poles  $\alpha(t)$ , using this method, have been made by zur Linden.<sup>6</sup> Earlier, less complete results were obtained by Chung and Snider<sup>7</sup> using the two-dimensional integral equation. We present in this paper some additional calculations of  $\alpha(t)$ , and also some

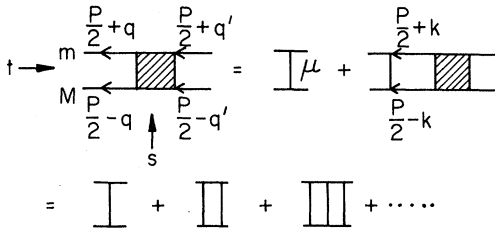


FIG. 1. The Feynman graphs for the Bethe-Salpeter equation in the ladder approximation.

new calculations of the residue functions  $\beta(t)$ . On the basis of our results we emphasize that even when the total energy does not vanish, it is still a good approximation to ignore the coupling between amplitudes for different four-dimensional spherical harmonics.

In addition, we consider the effect of corrections to the ladder approximation. The Bethe-Salpeter equation is exact if we include in the potential the sum of all two-particle irreducible Feynman graphs. A second term in this series is the crossed-box graph shown in Fig. 2. We present here some numerical calculations, including this term, of the Regge pole  $\alpha(0)$  as a function of the coupling constant.

A development very closely related to the Bethe-Salpeter equation is the multiperipheral model, invented in 1962 by Amati, Bertocchi, Fubini, Stanghellini, and Tonin<sup>8,9</sup> (ABFST). In its simplest form this model is described by the same set of graphs as in Fig. 1, with a different interpretation. For the Bethe-Salpeter equation, one thinks of a bound state or scattering state of the two particles forming the sides of the ladder; the rungs of the ladder represent the potential. For this case,  $t = (\text{energy})^2 > 0$ ,  $s = -(\text{momentum transfer})^2 < 0$ . In the multiperipheral model one deals with the absorptive part of the amplitude in the  $s$  channel. This is given by unitarity as a sum over  $n$ -particle intermediate states. The rungs of the ladder now represent the real on-shell particles in the  $n$ -particle intermediate state. For this case,  $s = (\text{energy})^2 > 0$ ,  $t = -(\text{momentum transfer})^2 \leq 0$ .

It is plausible that the Bethe-Salpeter and the multiperipheral approaches are related by an analytic continuation procedure, and this was proved by Bertocchi, Fubini, and Tonin<sup>8</sup> and Sertorio and Toller.<sup>10</sup> If one makes an  $O(3)$  decomposition of the Bethe-Salpeter equation and analytically continues to negative  $t$ , one obtains the same results as if one makes the appropriate  $O(2, 1)$  expansion on the multiperipheral equation. This whole subject of  $O(2, 1)$  and  $O(3, 1)$  expansions for the multiperipheral equation has been extensively studied recently by Ciafaloni and DeTar<sup>11</sup> and Saunders,

$$V = \text{I} + \text{II} + \dots$$

FIG. 2. The Feynman graphs for the two lowest-order terms in the potential for the Bethe-Salpeter equation.

Saxton, and Tan.<sup>12</sup> In the present paper we are not so much concerned with theoretical proofs, except insofar as they bear on the practical question of how to perform the numerical calculations in the most expeditious fashion. For this purpose, the  $O(4)$  decomposition discussed in the next section seems simplest and completely adequate. Thus, insofar as calculation of Regge poles is concerned, the Bethe-Salpeter and multiperipheral equations are identical.

In Sec. IV of this paper we consider the multiperipheral equation for the forward direction, where the absorptive part is proportional to the total cross section. For this case the equation can be transformed into a relatively simple two-dimensional integral equation of Volterra type. This equation can be numerically solved relatively easily by iteration. One knows from general principles that the iteration solution will converge. The important point for practical purposes is that it converges rapidly for reasonable values of  $s$ ; this is related to the fact that the average multiplicity for the multiperipheral model grows as  $\ln s$ . The solution of this integral equation gives directly the cross sections for  $n$ -particle production as a function of energy, and the total cross section as the sum of these. The solution contains the contributions from all Regge poles, not just the leading one. Thus, if some of the Regge poles are complex, as suggested recently,<sup>13,14</sup> the solution could show oscillations.

The plan of this paper is the following. In Sec. II we present the theoretical background for the Bethe-Salpeter equation. In Sec. III we give some numerical results obtained for Regge poles using the formulas of Sec. II. In Sec. IV we give the theoretical background for the form of the multiperipheral integral equation used to obtain the numerical results given in Sec. V. The theoretical Secs. II and IV are not very original. Most or all of this material is known to experts. We present it here to form a complete story and in an attempt to extract from the many complex papers on this subject the basic elements which are necessary for writing computer programs to solve the equations numerically.

## II. THE BETHE-SALPETER EQUATION

### A. The Ladder Approximation

The Bethe-Salpeter equation for the series of ladder graphs displayed in Fig. 1 is

$$T(q, q', P) = V(q, q') - i \int \frac{d^4 k}{(2\pi)^4} V(q, k) \times \frac{1}{(\frac{1}{2}P + k)^2 + m^2} \frac{1}{(\frac{1}{2}P - k)^2 + M^2} T(k, q', P), \tag{1}$$

with

$$V(q, q') = g^2 / [(q - q')^2 + \mu^2]. \tag{2}$$

The two particles which form the sides of the ladder have masses  $m$  and  $M$ , and the rungs of the ladder have mass  $\mu$ . We assume a scalar coupling with coupling constant  $g$  at each vertex. The energy squared in the center-of-mass system of the two particles  $m$  and  $M$  is

$$t = -P^2 = P_0^2 - \vec{P}^2.$$

We shall work in the center-of-mass system with  $\vec{P} = 0$ . It is more convenient to introduce a wave-function-like object

$$\psi(q, q', P) = \frac{1}{(\frac{1}{2}P + q)^2 + m^2} \frac{1}{(\frac{1}{2}P - q)^2 + M^2} T(q, q', P), \tag{3}$$

which then satisfies the equation

$$[(\frac{1}{2}P + q)^2 + m^2][(\frac{1}{2}P - q)^2 + M^2]\psi(q, q', P) = V(q, q') - i \int \frac{d^4 k}{(2\pi)^4} V(q, k)\psi(k, q', P). \tag{4}$$

This eliminates  $P$  from the kernel of the integral equation. In order to deal with the four-dimensional rotation group  $O(4)$  instead of the Lorentz group  $O(3, 1)$ , we make the Wick rotation<sup>15</sup> so that  $k_0$  is integrated up the imaginary axis, and then change variables,  $k_0 = ik_4$ :

$$\int d^4 k = \int d^3 k \int_{-\infty}^{\infty} dk_0 \Rightarrow \int d^3 k \int_{-i\infty}^{+i\infty} dk_0 = i \int d^3 k \int_{-\infty}^{\infty} dk_4. \tag{5}$$

A similar rotation and change of variables is made on  $q_0 = iq_4$ . It is easy to verify that the poles in the Feynman propagators in Eq. (1) (with the usual recipe  $m^2 \rightarrow m^2 - i\epsilon$ ,  $M^2 \rightarrow M^2 - i\epsilon$ ) do not interfere with the Wick rotation for  $\sqrt{s} < 2\min(m, M)$ . After this rotation, the Bethe-Salpeter equation assumes the form

$$(q^2 + m^2 - i\sqrt{t}q_4 - \frac{1}{4}t)(q^2 + M^2 + i\sqrt{t}q_4 - \frac{1}{4}t)\psi(q, q', P) = V(q, q') + \int \frac{d^4 k}{(2\pi)^4} V(q, k)\psi(k, q', P), \tag{6}$$

where  $q$  and  $k$  are now Euclidean four-vectors and,

e.g.,  $q^2 = \vec{q}^2 + q_4^2$ .

For  $t=0$  this equation is invariant with respect to four-dimensional rotations. For  $t \neq 0$  the terms  $\sqrt{t}q_4$  destroy the four-dimensional symmetry. We expand  $\psi$  in four-dimensional spherical harmonics. Then at  $t=0$  the equations for the different amplitudes decouple, and for  $t$  small the coupling between different amplitudes is small. The four-dimensional spherical harmonics, or hyperspherical harmonics, are the eigenfunctions of the angular part of the four-dimensional Laplacian in Euclidean space. They have the form

$$Z_{nlm_l}(\chi, \theta, \varphi) = D_{n-l}^{l+1}(\cos\chi) Y_l^{m_l}(\theta, \varphi), \quad l=0, 1, \dots, n. \tag{7}$$

Here  $\chi$  is the angle with the  $q_4$  axis and the  $D_{n-l}^{l+1}$  are normalized Gegenbauer functions,

$$D_{\lambda}^{l+1}(\cos\chi) = 2^l \Gamma(l+1) \left[ \frac{2\Gamma(\lambda+1)(l+\lambda+1)\sin^{2l}\chi}{\pi\Gamma(\lambda+2l+2)} \right]^{1/2} C_{\lambda}^{l+1}(\cos\chi), \tag{8}$$

$$\int_0^{\pi} \sin^2\chi d\chi D_{\mu}^{l+1}(\cos\chi) D_{\lambda}^{l+1}(\cos\chi) = \delta_{\mu\lambda}. \tag{9}$$

The functions  $C_{\lambda}^{l+1}(\cos\chi)$  are the Gegenbauer polynomials. The properties of these polynomials are given in well-known reference books.<sup>16,17</sup> From the identities to be found in these books it is easy to derive the useful relations

$$\cos\chi D_{\lambda}^{l+1}(\cos\chi) = A_{\lambda-1}^l D_{\lambda-1}^{l+1}(\cos\chi) + A_{\lambda}^l D_{\lambda+1}^{l+1}(\cos\chi), \tag{10}$$

$$A_{\lambda}^l = \frac{1}{2} \left[ \frac{(\lambda+1)(\lambda+2l+2)}{(\lambda+l+1)(\lambda+l+2)} \right]^{1/2},$$

and

$$\frac{1}{(q-k)^2 + \mu^2} = \frac{1}{2QK} \sum_{n=0}^{\infty} f_n \left( \frac{Q^2 + K^2 + \mu^2}{2QK} \right) C_n^1 \left( \frac{q \cdot k}{QK} \right) = \frac{\pi^2}{QK} \sum_{n=0}^{\infty} \sum_{l=0}^n \sum_{m_l=-l}^l \frac{1}{n+1} f_n \left( \frac{Q^2 + K^2 + \mu^2}{2QK} \right) \times Z_{nlm_l}(\chi_q, \theta_q, \varphi_q) Z_{nlm_l}^*(\chi_k, \theta_k, \varphi_k). \tag{11}$$

In this last identity,

$$f_n(x) = 2/[x + (x^2 - 1)^{1/2}]^{n+1}, \tag{12}$$

and we have used capital letters  $Q$  and  $K$  to stand for the lengths of the Euclidean four-vectors:

$$Q = (q^2)^{1/2} = (\vec{q}^2 + q_4^2)^{1/2}.$$

We now expand  $\psi(q, q', P)$  in the hyperspherical harmonics:

$$\psi(q, q', P) = \sum_{l=0}^{\infty} \sum_{n=l}^{\infty} \sum_{n'=l}^{\infty} \sum_{m_l=-l}^l \psi_{nm'}^l(Q, Q', t) Z_{n_1 m_1}(\chi_q, \theta_q, \varphi_q) Z_{n'_1 m'_1}^*(\chi_{q'}, \theta_{q'}, \varphi_{q'}). \quad (13)$$

Substituting the expansions (11) and (13) in the Bethe-Salpeter equation (6), and using  $q_4 = Q \cos \chi$  and the identity (10), we find the coupled equations for the amplitudes  $\psi_{nm'}^l(Q, Q', t)$ :

$$\begin{aligned} & \{ (Q^2 + m^2 - \frac{1}{4}t)(Q^2 + M^2 - \frac{1}{4}t) + tQ^2[(A_{n-l}^l)^2 + (A_{n-1-l}^l)^2] \} \psi_{nm'}^l(Q, Q', t) \\ & - i\sqrt{t}Q(M^2 - m^2)[A_{n-l}^l \psi_{n+1, n'}^l(Q, Q', t) + A_{n-1-l}^l \psi_{n-1, n'}^l(Q, Q', t)] \\ & + tQ^2[A_{n+1-l}^l A_{n-l}^l \psi_{n+2, n'}^l(Q, Q', t) + A_{n-2-l}^l A_{n-1-l}^l \psi_{n-2, n'}^l(Q, Q', t)] \\ & = (2\pi)^4 \delta_{n, n'} V_n(Q, Q') + \int_0^\infty K^3 dK V_n(Q, K) \psi_{nm'}^l(K, Q', t), \quad (14) \end{aligned}$$

where

$$V_n(Q, K) = \frac{g^2}{16\pi^2} \frac{1}{n+1} \frac{1}{QK} f_n \left( \frac{Q^2 + K^2 + \mu^2}{2QK} \right). \quad (15)$$

Equation (14) and its interpretation are rather well known.<sup>4-7</sup> The equation is analytically continued to nonintegral  $n$  and  $l$  keeping  $n-l = \text{integer}$ . Since  $V_n(Q, K)$  depends only on  $n$ , not  $l$ , at  $t=0$  the equations for the  $\psi_{nm'}^l(Q, Q', 0)$  decouple from each other and there is no dependence on  $l$ . A Regge pole at  $l=n$  implies then a series of daughter poles at  $l=n-1, n-2, \dots$ . For  $t \neq 0$  there is some coupling between different amplitudes and some dependence on  $l$ ; there will still be sequences of daughter poles, but the spacing between trajectories is no longer unity. Note that there is a substantial simplification in Eq. (14) if the masses on the two sides of the ladder are equal. In this case there is coupling only between  $\psi_{nm'}^l$  with  $n$ 's differing by a multiple of 2. We present some numerical solutions of Eq. (14) for Regge poles in the next section.

### B. The Crossed-Box Potential

The Bethe-Salpeter equation is a rigorous equation if one includes in the potential  $V$  the sum of

all two-particle irreducible graphs. In the discussion above we have kept only the lowest-order contribution to the potential, the single rung of the ladder. A second contribution to the potential is the crossed-box graph displayed in Fig. 2. It is feasible to include this contribution to the potential in numerical calculations, and it is of some interest to see by how much numerical results are changed when this second-order contribution to the potential is included. Accordingly, we derive here the formula from which this second-order potential can be calculated. Unlike the lowest-order potential discussed above, the crossed-box potential depends on the total energy-momentum vector  $P$ . In what follows we shall neglect this dependence by setting  $P=0$  in the crossed-box potential. We shall also assume the masses on the two sides of the ladder are equal,  $m=M$ . The momentum labels are then as indicated in Fig. 3. The graph of Fig. 3 is invariant with respect to the interchange  $q \rightarrow -q$ , i.e., with respect to the interchange of the Mandelstam variables  $s$  and  $u$ , where  $s+t+u=2Q^2+2K^2=\Sigma$ . The dispersion relation for the crossed-box potential at  $t=0$  is then

$$V_2(q, k) = V_2(s, u) = \frac{1}{\pi} \int_{4\mu^2}^{\infty} ds' \text{Im} V_2(s', \Sigma - s') \left( \frac{1}{s' - s} + \frac{1}{s' - u} \right). \quad (16)$$

Using the formula (11) we find

$$\frac{1}{s' - s} = \frac{1}{s' + (q - k)^2} = \frac{\pi^2}{QK} \sum_{n, m_1} \frac{1}{n+1} f_n \left( \frac{Q^2 + K^2 + s'}{2QK} \right) Z_{n_1 m_1}(q) Z_{n_1 m_1}^*(k), \quad (17)$$

$$\frac{1}{s' - u} = \frac{1}{s' + (q + k)^2} = \frac{\pi^2}{QK} \sum_{n, m_1} \frac{(-1)^n}{n+1} f_n \left( \frac{Q^2 + K^2 + s'}{2QK} \right) Z_{n_1 m_1}(q) Z_{n_1 m_1}^*(k). \quad (18)$$

Substituting these in (16), we find

$$V_2(q, k) = \frac{\pi^2}{QK} \sum_{n, m_1} \frac{1 + (-1)^n}{n+1} Z_{n_1 m_1}(q) Z_{n_1 m_1}(k) \frac{1}{\pi} \int_{4\mu^2}^{\infty} ds' \text{Im} V_2(s', \Sigma - s') f_n \left( \frac{Q^2 + K^2 + s'}{2QK} \right). \quad (19)$$

The factor  $\text{Im} V_2(s, \Sigma - s)$  in the integrand is given by a two-particle unitarity calculation. Working in the

center-of-mass system in the  $s$  channel (see Fig. 3) and with  $p$  and  $q$  standing for the magnitudes of three-vectors in (20), we find

$$\begin{aligned} \text{Im} V_2(s, \Sigma - s) &= \frac{p}{2(4\pi)^2 \sqrt{s}} 2\pi \int_{-1}^1 d(\cos \theta) \frac{g^2}{q^2 + p^2 - (E_q - E_p)^2 + m^2 - 2pq \cos \theta} \frac{1}{q^2 + p^2 - (E_k - E_p)^2 + m^2 + 2pq \cos \theta} \\ &= \frac{g^4}{8\pi} \frac{1}{[s^2 + 2s(Q^2 + K^2) + (Q^2 - K^2)^2]^{1/2}} \frac{1}{s + Q^2 + K^2 - 2\mu^2 + 2m^2} \ln \frac{1+X}{1-X}, \end{aligned} \tag{20}$$

$$X = \frac{(s - 4\mu^2)^{1/2} [s^2 + 2s(Q^2 + K^2) + (Q^2 - K^2)^2]^{1/2}}{\sqrt{s}(s + Q^2 + K^2 - 2\mu^2 + 2m^2)}.$$

In the numerical calculations reported in the next section the integral in (19) is evaluated numerically using the explicit formula (20) for  $\text{Im} V_2(s', \Sigma - s')$ .

C. The Residue Function

As a final topic in this section, we formulate more exactly the mathematical problem of finding a Regge pole, and in particular we show how to calculate the residue of the pole. Suppose we write the coupled Eqs. (14), in a very compressed matrix notation, in the form

$$K\psi = V + V\psi. \tag{21}$$

The  $T$ -matrix-like quantity corresponding to the wave-function-like quantity  $\psi$  is given by

$$T = K\psi \tag{22}$$

and satisfies the equation

$$T = V + V \frac{1}{K} T. \tag{23}$$

At a Regge pole, which in the present context we may think of as a bound state at a not necessarily integral  $l$ , we have  $T$  and  $\psi \rightarrow \infty$ , and so  $\psi$  satisfies the homogeneous equation

$$K\psi = V\psi. \tag{24}$$

The parameters describing the Regge pole are determined then by the condition that (24) have a

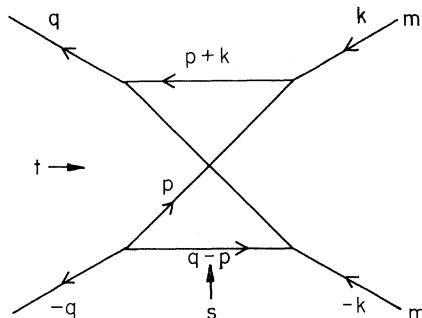


FIG. 3. The second-order crossed-box potential for the Bethe-Salpeter equation.

nontrivial solution:

$$\det[K - V] = 0. \tag{25}$$

This equation determines one of the three quantities  $t$ ,  $g$ , and  $l = \alpha(t)$  in terms of the other two.

We can now set up a new and somewhat artificial eigenvalue problem with the parameters determined by (25) held fixed:

$$\lambda_i K \psi_i = V \psi_i. \tag{26}$$

We suppose that  $\lambda_1 = 1$ ,  $\psi_1 = \psi$  are the eigenvalue and eigenfunction determined in (24), (25). Accompanying this eigenvalue and eigenfunction are an infinite set of eigenvalues  $\lambda_i$  and eigenfunctions  $\psi_i$ , the latter assumed to form a complete set. Thus

$$\lambda_1(\alpha(t)) = 1. \tag{27}$$

If we now change slightly the value of  $l$  in  $K$  and  $V$ ,  $\lambda_1$  will change slightly:

$$\lambda_1(l) = 1 + \lambda_1'(\alpha(t))[l - \alpha(t)] + \dots \tag{28}$$

Now, if  $M$  is a matrix with eigenvalues  $\lambda_i$  and eigenfunctions  $\psi_i$ ,

$$M \psi_i = \lambda_i \psi_i, \tag{29}$$

the transpose matrix  $\bar{M}$  will have the same eigenvalues but different eigenfunctions,

$$\bar{M} \varphi_i = \lambda_i \varphi_i. \tag{30}$$

From (30),

$$\bar{\varphi}_i M = \lambda_i \bar{\varphi}_i, \tag{31}$$

and from (29) and (31) we obtain an orthogonality relation,

$$(\lambda_i - \lambda_j)(\bar{\varphi}_i \psi_j) = 0. \tag{32}$$

This implies a completeness relation,

$$1 = \sum_i \frac{\psi_i \bar{\varphi}_i}{(\bar{\varphi}_i \psi_i)}, \tag{33}$$

and the expansion

$$\frac{1}{1-M} = \sum_i \frac{1}{1-\lambda_i} \frac{\psi_i \bar{\varphi}_i}{(\bar{\varphi}_i \psi_i)}. \quad (34)$$

Applying this to Eq. (26),

$$M = \frac{1}{K} V, \quad (35)$$

$$\tilde{M} = V \frac{1}{K}, \quad (36)$$

since  $\tilde{V} = V$  and  $\tilde{K} = K$  according to Eqs. (14) and (15). Comparing (35) and (36) with (29) and (30), we find

$$\varphi_i = K \psi_i = \frac{1}{\lambda_i} V \psi_i. \quad (37)$$

Manipulating Eq. (23), we obtain

$$T = \frac{1}{1-VK^{-1}} V = \frac{1}{V^{-1}-K^{-1}} = V \frac{1}{1-K^{-1}V}. \quad (38)$$

Using (34) and (36), this can be rewritten in the form

$$\begin{aligned} T &= V \frac{1}{1-K^{-1}V} \sum_i \frac{\psi_i \bar{\varphi}_i}{(\bar{\varphi}_i \psi_i)} \\ &= V \sum_i \frac{1}{1-\lambda_i} \frac{\psi_i \bar{\varphi}_i}{(\bar{\varphi}_i \psi_i)} \\ &= \sum_i \frac{1}{(1-\lambda_i)\lambda_i} \frac{V \psi_i \bar{\psi}_i V}{(\bar{\psi}_i K \psi_i)}. \end{aligned} \quad (39)$$

Using (28) and keeping only the one term  $i=1$  in the neighborhood of the Regge pole, we find

$$T = \frac{1}{l-\alpha(t)} \left( \frac{-1}{\lambda_1'(\alpha(t))} \right) \frac{V \psi_1 \bar{\psi}_1 V}{(\bar{\psi}_1 K \psi_1)}. \quad (40)$$

This formula provides a practical way of computing the residue of the Regge pole. The elements of the column vector  $\psi_1$  are obtained from (24) once (25) has been satisfied. [One should note in this connection a confusing point about our notation. The  $\psi_{nm}'(Q, Q')$  of Eq. (14) depend on two sets of variables  $n, Q$  and  $n', Q'$ . The  $\psi_i$  of (26), and in particular  $\psi_1$  used in (40), are true wave functions for a bound state and depend on only one set of variables  $n, Q$ .] In the numerator of Eq. (40) the quantity  $V\psi_1$  is the integral on the right side of (14). Also, we must analytically continue to the mass shell for the two external particles:

$$\left(\frac{1}{2}P+q\right)^2 + m^2 = \left(\frac{1}{2}P-q\right)^2 + m^2 = 0,$$

or

$$q^2 = Q^2 = \frac{1}{4}(t - 4m^2), \quad (41)$$

$$P \cdot q = i\sqrt{t} Q \cos \chi = 0. \quad (42)$$

With  $t < 4m^2$ ,  $Q$  is pure imaginary,

$$Q = iQ_m = \frac{1}{2}i(4m^2 - t)^{1/2}. \quad (43)$$

The argument of the function  $f_n(x)$  in  $V_n(Q, K)$  then

becomes

$$x = \frac{Q^2 + K^2 + \mu^2}{2QK} = -i \frac{-Q_m^2 + K^2 + \mu^2}{2Q_m K} \equiv -ix', \quad (44)$$

and

$$\begin{aligned} f_n(x) &= \frac{2}{(-i)^{n+1} [x' + (x'^2 + 1)^{1/2}]^{n+1}} \\ &\equiv \frac{1}{(-i)^{n+1}} \mathfrak{F}_n(x'). \end{aligned} \quad (45)$$

Putting all this into (40) and rewriting that formula in detail, including a factor  $(2\pi)^4$  from (14), we find

$$T_{nn'}^l = e^{-i\pi\alpha(t)} \frac{R_{nn'}^l}{l-\alpha(t)}, \quad (46)$$

where

$$R_{nn'}^l = (-1)^{(n-l+n'-l)/2} \left( -\frac{1}{\lambda_1'(\alpha(t))} \right) (2\pi)^4 \frac{N_n N_{n'}}{D} \quad (47)$$

and

$$N_n = \int_0^\infty K^3 dK \frac{g^2}{16\pi^2} \frac{1}{n+1} \frac{1}{Q_m K} \mathfrak{F}_n \left( -\frac{Q_m^2 + K^2 + \mu^2}{2Q_m K} \right) \psi_n^l(K), \quad (48)$$

$$D = \sum_{n, n'=l}^\infty \int_0^\infty Q^3 dQ \psi_n^l(Q) K_{nn'}^l(Q) \psi_{n'}^l(Q). \quad (49)$$

In these formulas  $\psi_n^l(K)$  is the solution of (24) and  $K_{nn'}^l(Q)$  is the matrix operator which appears on the left of (14). In using these formulas we recall that while  $n$  and  $l$  are not necessarily integral,  $n-l$  is integral and in fact an even integer,  $n-l=0, 2, 4, \dots$  for the equal-mass case under consideration. Carrying out the summation over  $m_i$  we can obtain the usual partial-wave expansion from an expansion of the type (13),

$$\begin{aligned} T(q, q', P) &= \sum_{i=0}^\infty \sum_{n=i}^\infty \sum_{n'=i}^\infty \sum_{m_i=-i}^i T_{nn'}^i Z_{n i m_i}(q) Z_{n' i m_i}(q') \\ &= \sum_i (2i+1) T_i P_i(\cos \theta_i), \end{aligned} \quad (50)$$

where

$$T_i = \frac{1}{4\pi} \sum_{n, n'=i}^\infty D_{n-i}^{i+1}(0) T_{nn'}^i D_{n'-i}^{i+1}(0). \quad (51)$$

The vanishing arguments for the functions  $D_{n-i}^{i+1}(\cos \chi)$  follow from the mass-shell conditions (42). Finally we recall that what we want to do with this Regge pole once we find it is put it in the series (50), perform the Sommerfeld-Watson transformation, and consider the behavior for large  $s$ . What will occur is then

$$\begin{aligned} P_{\alpha(t)}(-\cos \theta_t) &= P_{\alpha(t)} \left( \frac{s-u}{4Q_m^2} \right) \\ &\xrightarrow{s \rightarrow \infty} \frac{\Gamma(2\alpha+1)}{2^{2\alpha} \Gamma^2(\alpha+1)} \left( \frac{s}{Q_m^2} \right)^{\alpha(t)}. \end{aligned} \quad (52)$$

We thus introduce a reduced residue function with the factor  $Q_m^{2\alpha}$  divided out,

$$T_l = e^{-i\pi\alpha(t)} Q_m^{2\alpha(t)} \frac{\beta_r(t)}{l - \alpha(t)}, \quad (53)$$

$$\beta_r(t) = \frac{1}{4\pi Q_m^{2\alpha(t)}} \sum_{n, n'=l}^{\infty} D_{n-l}^{l+1}(0) R_{nn'}^l D_{n'-l}^{l+1}(0). \quad (54)$$

For large  $s$ , the total cross section in the  $s$  channel is then given by

$$\begin{aligned} \sigma_{\text{tot}}(s) &= \frac{1}{s} \text{Im} T(s, 0) \\ &= \pi(2\alpha + 1) \frac{\Gamma(2\alpha + 1)}{2^{2\alpha} \Gamma^2(\alpha + 1)} \beta_r(0) s^{\alpha-1}, \quad \alpha = \alpha(0). \end{aligned} \quad (55)$$

$$\begin{aligned} &\left\{ \left( 1 - \frac{t}{4(Q^2 + m^2)} \right)^2 + t \frac{Q^2}{(Q^2 + m^2)^2} [(A_{n-l}^l)^2 + (A_{n-1-l}^l)^2] \right\} \psi_n^{l'}(Q) + t \frac{Q^2}{(Q^2 + m^2)^2} [A_{n+1-l}^l A_{n-l}^l \psi_{n+2}^{l'}(Q) + A_{n-2-l}^l A_{n-1-l}^l \psi_{n-2}^{l'}(Q)] \\ &= \int_0^{\infty} K^3 dK V_n(Q, K) \frac{1}{(K^2 + m^2)^2} \psi_n^{l'}(K). \end{aligned} \quad (57)$$

In these equations the integrals are replaced by sums using Gaussian quadrature mesh points. In this way the integral equations are replaced by matrix equations. The eigenvalue equation is the usual condition that the set of homogeneous linear equations have a nontrivial solution, as indicated in Eq. (25). There are three parameters in these equations:  $t$ ,  $g$ , and  $l = \alpha(t)$ . If two of these are given, the remaining one is determined by Eq. (25).

Thus, if we want a Pomeranchuk pole at  $\alpha(0) = 1$  for  $t=0$ ,  $g$  is determined. In fact, for  $M=m=\mu$ ,  $g^2/16\pi^2 m^2$  is determined to be 16.38. With this coupling constant we can now determine the Regge trajectories and residue functions as a function of  $t$ . Some results for the trajectories obtained in this case are presented in Fig. 4; in Fig. 5 we give the reduced residue function of Eqs. (53), (54). The trajectories in Fig. 4 have been obtained previously by Chung and Snider<sup>7</sup> and zur Linden.<sup>6</sup> In addition to the leading Pomeranchuk trajectory, there is a daughter trajectory which passes through  $\alpha=0$  at  $t=0$ , and a secondary trajectory nearly degenerate with the daughter. The wave function for the leading Pomeranchuk trajectory has no nodes, as does the wave function for the daughter trajectory. The wave function for the secondary trajectory has one node. The reduced residue functions for the leading Pomeranchuk trajectory and the secondary trajectory are given in Fig. 5. For the daughter trajectory the residue function vanishes identically. [In Eq. (54) the functions  $D_{n-l}^{l+1}(0)$  vanish identically for  $n-l = \text{odd integer}$ .]

The point we would like to emphasize in connection with Figs. 4 and 5 is the high accuracy of the approximation of neglecting the coupling between

### III. NUMERICAL RESULTS FOR THE BETHE-SALPETER EQUATION

In this section we record some numerical results for Regge-pole parameters obtained by numerical solution of Eq. (14). We consider only the equal-mass case  $M=m$ . For practical purposes it is convenient to introduce a new wave function

$$\psi_n^{l'} = (Q^2 + m^2)^2 \psi_n^l. \quad (56)$$

The Regge pole is found from the homogeneous equation obtained by dropping the inhomogeneous term in Eq. (14):

components of the wave function with different values of the  $O(4)$  quantum number  $n$ . Of course at  $t=0$  the equations decouple completely. However, for  $|t/m^2|$  as large as 2 it is a very good approximation to neglect the second group of terms in Eq. (57) in which  $\psi_n^{l'}$  is coupled to  $\psi_{n\pm 2}^{l'}$ . This was tested by writing the program in such a way that the number of amplitudes coupled together could be varied. It was found that coupling three successive values of  $n$  ( $n, n+2, n+4$ ) gave essentially exact results out to  $|t/m^2| \approx 2$ . For the trajectories in Fig. 4 the difference between the results obtained with decoupled equations (just one  $n$  value) and the exact results is so small as to be difficult to plot - less than a few percent. The differences are larger for the residue functions plotted in Fig. 5. Here the smooth curves give the exact results, and the dashed curves the results with decoupled equations. It is seen that the decoupled approximation is adequate except when very accurate numerical results are desired. It seems to the present writer that the accuracy of the decoupled approximation is an important point which may be useful in other calculations more realistic and extensive than any attempted here. Mathematically, the decoupling amounts to replacing a two-dimensional integral equation by a one-dimensional one, a very significant simplification.

In Fig. 6 we present some Regge trajectories for a different choice of masses. The sides of the ladder are taken to have the pion mass and the rungs to have the mass of the  $\rho$  meson. The couplings are all taken to be scalar. For  $g^2/16\pi^2 = 3.182 \text{ GeV}^2$  the trajectory passes through  $\alpha(0) = 1$ . For  $g^2/16\pi^2 = 1.143 \text{ GeV}^2$  it passes through  $\alpha(0) = \frac{1}{2}$ .

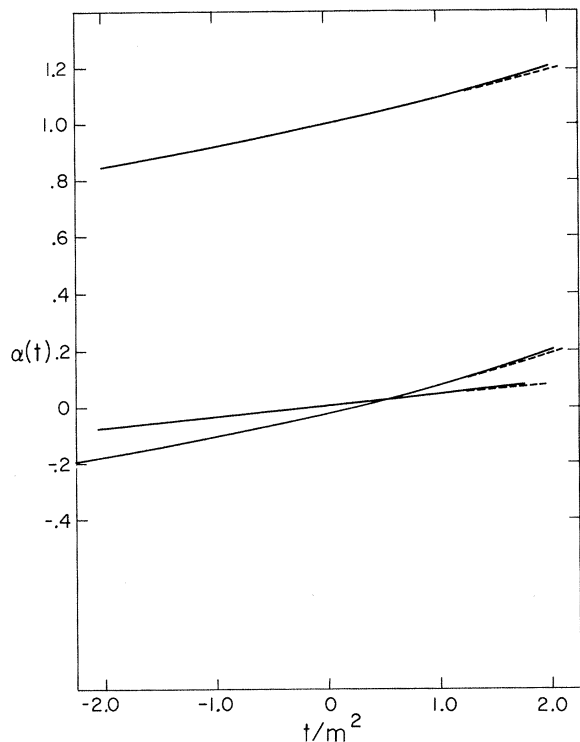


FIG. 4. The Regge trajectories obtained from the Bethe-Salpeter equation in the ladder approximation with all masses equal:  $\mu = m$ ,  $g^2/16\pi^2 m^2 = 16.38$ . The solid curves are exact results. The dashed curves are obtained by neglecting the coupling between  $O(4)$  states.

The complete trajectories for these two choices of coupling constants are given in Fig. 6. In Fig. 7 we give the reduced residue functions corresponding to the trajectories in Fig. 6. The residue functions are almost constant in this case. Again, the exact results given in the figures by the solid curves differ at most by a few percent from the results obtained by decoupling the equations and keeping only one  $n$  value, the dashed curves.

In Fig. 8 we fix  $t=0$  and plot as a function of  $\alpha(0)$  the coupling constant necessary to produce a Regge pole with intercept  $\alpha(0)$ . This calculation was made for the case  $M=m=\mu$ . The upper curve was obtained with the lowest-order potential (2). The middle curve was obtained with a potential consisting of the sum of (2) and (19) (see Fig. 2). The bottom curve is the perturbation-theory result for  $\alpha(0)$ ,

$$\alpha(0) = -1 + g^2/16\pi^2 m^2.$$

The curves in Fig. 8 speak for themselves. It is seen that for large  $\alpha(0)$  the curves differ considerably. Presumably, the inclusion of other terms in the potential will produce similarly large changes. It is seen that the perturbation-theory formula used in recent eikonal calculations<sup>18</sup> is not at all accurate near  $\alpha(0) = 1$ .

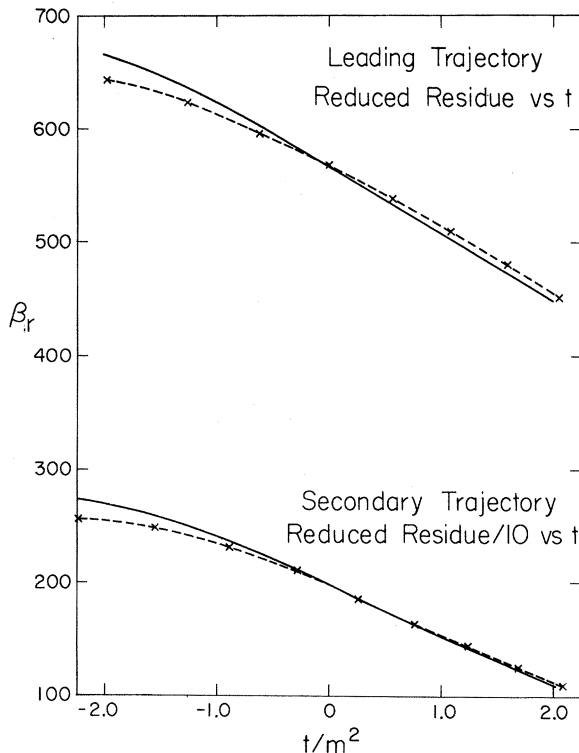


FIG. 5. The reduced residue functions obtained from the Bethe-Salpeter equation in the ladder approximation with all masses equal:  $\mu = m$ ,  $g^2/16\pi^2 m^2 = 16.38$ . The solid curves are exact results. The dashed curves are obtained by neglecting the coupling between  $O(4)$  states. The units of  $\beta_r$  are  $(\text{GeV})^{-2\alpha(t)}$ , where  $\alpha(t)$  is given in Fig. 4.

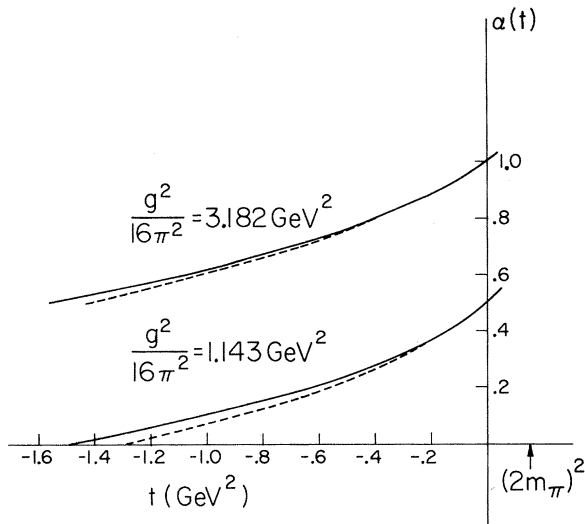


FIG. 6. Regge trajectories obtained from the Bethe-Salpeter equation in the ladder approximation when the sides of the ladder have the pion mass and the rungs have the  $\rho$ -meson mass. The trajectories are given for two choices of coupling constant. The solid curves are exact results. The dashed curves are obtained by neglecting the coupling between  $O(4)$  states.

IV. THE ABFST EQUATION

This famous equation is closely related to the Bethe-Salpeter equation (1). Referring to Fig. 1, we suppose  $s > 0$ ,  $t < 0$  and calculate the absorptive part of the invariant amplitude in the  $s$  channel, using unitarity:

$$\text{Im}T_{ij} = \frac{1}{2} \sum_n (2\pi)^4 \delta(p_i - p_n) \frac{T_{in} T_{jn}^*}{\pi(2E)_n} \tag{58}$$

This sum over  $n$ -particle intermediate states is the iteration solution of the ABFST equation. With  $A = \text{Im}T$  we find

$$A(q, q', P) = g^2 \pi \delta((q - q')^2 + \mu^2) + \int \frac{d^4k}{(2\pi)^4} g^2 2\pi \delta((q - k)^2 + \mu^2) \frac{1}{(\frac{1}{2}P + k)^2 + m^2} \frac{1}{(\frac{1}{2}P - k)^2 + M^2} A(k, q', P). \tag{59}$$

Much has been written in recent times on the problem of making appropriate  $O(2, 1)$  or  $O(3, 1)$  expansions of this equation so as to obtain equations determining the Regge poles.<sup>11, 12</sup> We do not wish to enter into that here. As explained in the introduction, at the numerical level, which is of most concern to us in this paper, the results must be the same as obtained in the previous sections. For such mundane purposes the methods discussed in Sec. II seem simplest and completely adequate.

We discuss in this section a slightly different approach which seems useful for some purposes and is numerically simple. First, we restrict ourselves to the forward direction in the  $s$  channel for equal-mass particles, i.e.,  $t = 0$  for  $m = M$ . The absorptive part is then simply related to the total cross section

$$A = 2p\sqrt{s}\sigma, \tag{60}$$

with  $p$  the center-of-mass momentum in the  $s$  channel. We can reverse the direction of some of the arrows in Fig. 1 so as to obtain Fig. 9. In terms of the notation introduced in this figure, we can transform the integration in Eq. (59) so that it assumes the form of a two-body phase-space calculation:

$$\begin{aligned} & \int \frac{d^4k}{(2\pi)^4} 2\pi \delta((q - k)^2 + \mu^2) \dots \\ &= \frac{1}{(2\pi)^3} \int ds' \int d^4q_1 \int d^4q_2 \delta(q_1^2 + \mu^2) \delta(s' + q_2^2) \delta^4(q_1 + q_2 - q - q') \dots \\ &= \frac{1}{(2\pi)^3} \int ds' \int \frac{d^3q_1}{2E_1} \int \frac{d^3q_2}{2E_2} \delta^4(q_1 + q_2 - q - q') \dots \\ &= \frac{1}{(2\pi)^3} \int ds' \int \sin\theta_1 d\theta_1 d\varphi_1 \frac{q_1^2}{2E_1 2E_2} \frac{dq_1}{d(E_1 + E_2)} \dots \\ &= \frac{1}{16\pi^2} \int ds' \int d\cos\theta_1 \frac{q_1}{\sqrt{s}} \dots \end{aligned} \tag{61}$$

For  $P = 0$  or  $t = 0$ , the  $\varphi_1$  integration just gives a factor  $2\pi$ . In the last two lines of Eq. (61)  $q_1$  stands for the magnitude of the center-of-mass momentum in the intermediate state in the  $s$  channel,

$$q_1 = \frac{[s^2 - 2s(s' + \mu^2) + (s' - \mu^2)^2]^{1/2}}{2\sqrt{s}}. \tag{62}$$

We can also introduce the center-of-mass momentum in the initial or final states in the  $s$  channel,

$$p = \frac{[s^2 + 2s(q^2 - m^2) + (q^2 + m^2)^2]^{1/2}}{2\sqrt{s}}. \tag{63}$$

In terms of  $p$  and  $q_1$  the scattering angle  $\theta_1$  to the intermediate state in Fig. 9 is given by

$$4pq_1 \cos\theta_1 = -2k^2 + s + q^2 - m^2 - \mu^2 - s' + (m^2 + q^2)(s' - \mu^2)/s. \tag{64}$$

Using Eq. (64) the integral over  $\cos\theta_1$  in Eq. (61) can be transformed into an integral over  $k^2$ . Substituting all these results back into (59), we find that the ABFST equation can be written in the form

$$A(s, q^2) = g^2 \pi \delta(s - \mu^2) + \frac{g^2}{16\pi^2} \frac{1}{[s^2 + 2s(q^2 - m^2) + (q^2 + m^2)^2]^{1/2}} \int_0^{(\sqrt{s-\mu})^2} ds' \int_{k_{\min}^2}^{k_{\max}^2} dk^2 \frac{A(s', k^2)}{(k^2 + m^2)^2}. \tag{65}$$

The limits on the  $k^2$  integration are obtained from Eq. (64) by setting  $\cos\theta_1 = \pm 1$ :

$$\begin{aligned} \left( \begin{array}{c} k_{\max}^2 \\ k_{\min}^2 \end{array} \right) &= \frac{1}{2} \left[ s + q^2 - m^2 - \mu^2 - s' + \frac{(q^2 + m^2)(s' - \mu^2)}{s} \right] \\ &\pm \frac{1}{2s} \{ [s^2 + 2s(q^2 - m^2) + (q^2 + m^2)^2][s^2 - 2s(s' + \mu^2) + (s' - \mu^2)^2] \}^{1/2}. \end{aligned} \quad (66)$$

The limit on the  $s'$  integration is the maximum  $s'$  consistent with conservation of energy. We can iterate Eq. (65) once and obtain

$$A(s, q^2) = g^2 \pi \delta(s - \mu^2) + B(s, q^2), \quad (67)$$

with  $B(s, q^2)$  satisfying

$$B(s, q^2) = B_2(s, q^2) + \frac{g^2}{16\pi^2} \frac{1}{[s^2 + 2s(q^2 - m^2) + (q^2 + m^2)^2]^{1/2}} \int_{4\mu^2}^{(s-\mu)^2} ds' \int_{k_{\min}^2}^{k_{\max}^2} dk^2 \frac{B(s', k^2)}{(k^2 + m^2)^2}. \quad (68)$$

The inhomogeneous term (the absorptive part of the box diagram) is given by

$$B_2(s, q^2) = \frac{g^4}{16\pi^2} \frac{(s - 4\mu^2)^{1/2}}{\sqrt{s}} [m^2 s + \mu^2 q^2 + \mu^4 - 3m^2 \mu^2 + s^{-1} \mu^2 (q^2 + m^2)^2]^{-1}. \quad (69)$$

The ABFST equation in the form (68), (69) forms the starting point for an investigation by Tiktopoulos and Treiman.<sup>19</sup>

#### V. NUMERICAL RESULTS FOR ABFST EQUATION

The ABFST equation in the form (68) is relatively easy to solve numerically. Since the equation is of Volterra type, the iteration solution converges. Furthermore, as has been known since the time of the original papers,<sup>9</sup> the expectation value for the number of particles grows logarithmically with  $s$ :

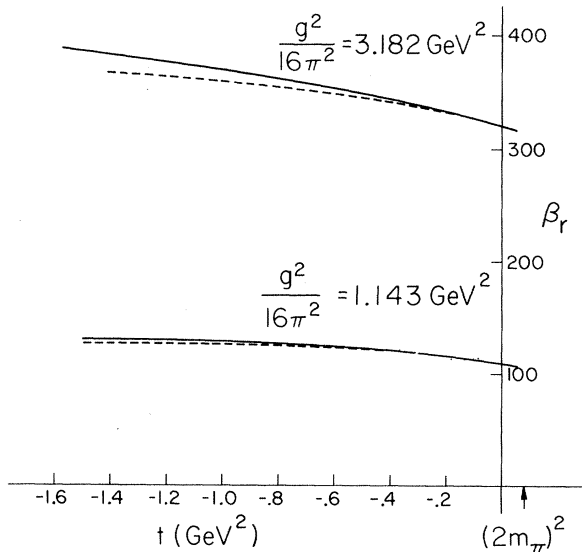


FIG. 7. The reduced residue functions obtained from the Bethe-Salpeter equation in the ladder approximation when the sides of the ladder have the pion mass and the rungs have the  $\rho$ -meson mass. The solid curves are exact results. The dashed curves are obtained by neglecting the coupling between  $O(4)$  states. The units of  $\beta_r$  are  $(\text{GeV})^{-2\alpha(t)}$ , where  $\alpha(t)$  is given in Fig. 6.

$\bar{n} = c \log s$ , and thus for any reasonable value of  $s$ ,  $\bar{n}$  is a small number,  $\bar{n} < 10$ , say. This means that the number of iterations necessary to achieve a high accuracy is much less than the number of iterations kinematically allowed by the value of  $s$ .

We present in Fig. 10 some numerical results obtained by straightforward numerical iteration of Eq. (68). We chose the case in which the exchanged particles (the sides of the ladder) have the pion mass and the produced particles (the rungs of the ladder) have the  $\rho$ -meson mass. The coupling constant was chosen to have the value  $g^2/16\pi^2 = 3.182$

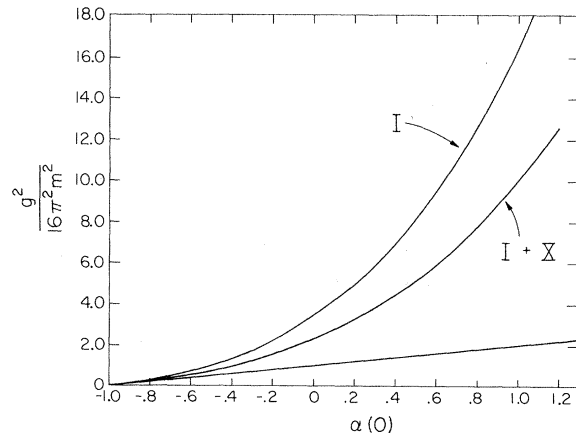


FIG. 8. The coupling constant  $g^2/16\pi^2 m^2$  vs  $\alpha(0)$  for the Bethe-Salpeter equation in the ladder approximation with all masses equal:  $\mu = m$ . The top curve is obtained in the ladder approximation. The middle curve is obtained for a potential consisting of the sum of the ladder potential, Eq. (2), and the crossed-box potential, Eq. (19). The bottom curve is the lowest-order perturbation-theory result.



\*Work supported in part by the National Science Foundation under Contract No. NSF GP 25303.

<sup>1</sup>E. E. Salpeter and H. A. Bethe, *Phys. Rev.* **84**, 1232 (1951).

<sup>2</sup>N. Nakanishi, *Progr. Theoret. Phys. (Kyoto) Suppl.* **43**, 1 (1969). This extensive review article contains many additional references.

<sup>3</sup>B. W. Lee and R. F. Sawyer, *Phys. Rev.* **127**, 2266 (1962).

<sup>4</sup>G. Domokos and P. Suranyi, *Nucl. Phys.* **54**, 529 (1964); G. Domokos, *Phys. Rev.* **159**, 1387 (1967).

<sup>5</sup>D. Z. Freedman and J. M. Wang, *Phys. Rev.* **153**, 1596 (1967).

<sup>6</sup>E. zur Linden, *Nuovo Cimento* **63A**, 181 (1969).

<sup>7</sup>V. Chung and D. R. Snider, *Phys. Rev.* **162**, 1639 (1967).

<sup>8</sup>L. Bertocchi, S. Fubini, and M. Tonin, *Nuovo Cimento* **25**, 626 (1962).

<sup>9</sup>D. Amati, A. Stanghellini, and S. Fubini, *Nuovo Cimento* **26**, 896 (1962).

<sup>10</sup>L. Sertorio and M. Toller, *Nuovo Cimento* **33**, 413 (1964).

<sup>11</sup>M. Ciafaloni and C. DeTar, *Phys. Rev. D* **1**, 2917 (1970).

<sup>12</sup>L. M. Saunders, O. H. N. Saxton, and C. I. Tan, *Phys. Rev. D* **3**, 1005 (1971).

<sup>13</sup>G. F. Chew and D. R. Snider, *Phys. Letters* **31B**, 75 (1970).

<sup>14</sup>M. L. Goldberger, D. Silverman, and C. I. Tan, *Phys. Rev. Letters* **26**, 100 (1971).

<sup>15</sup>G. C. Wick, *Phys. Rev.* **96**, 1124 (1954).

<sup>16</sup>W. Magnus and F. Oberhettinger, *Formulas and Theorems for the Functions of Mathematical Physics* (Chelsea, New York, 1949), p. 76.

<sup>17</sup>*Higher Transcendental Functions*, edited by A. Erdélyi *et al.* (McGraw-Hill, New York, 1953), Vol. I, p. 175.

<sup>18</sup>S. J. Chang and T. M. Yan, *Phys. Rev. Letters* **25**, 1586 (1970); B. Hasslacher, D. K. Sinclair, G. M. Cicuta, and R. L. Sugar, *ibid.* **25**, 1591 (1970).

<sup>19</sup>G. Tiktopoulos and S. B. Treiman, *Phys. Rev.* **135**, B711 (1964).

<sup>20</sup>M. N. Misheloff, *Phys. Rev. D* **3**, 1486 (1971).

<sup>21</sup>Sun-Sheng Shei, *Phys. Rev. D* **3**, 1962 (1971).

PHYSICAL REVIEW D

VOLUME 3 NUMBER 12

15 JUNE 1971

## Sixth-Order Radiative Corrections to the Anomalous Magnetic Moment of the Electron

J. Calmet

*Department of Physics, University of Utah, Salt Lake City, Utah 84112  
and Centre de Physique Théorique, Centre National de la Recherche Scientifique, Marseille, France*

and

M. Perrottet

*Centre de Physique Théorique, Centre National de la Recherche Scientifique, Marseille, France*

(Received 31 August 1970)

In order to evaluate the contributions to the anomalous magnetic moment of the electron ( $a_e$ ), a method entirely based on computer techniques is developed. This method is embedded in the framework of the functional formalism. As a first result, the contributions to the  $\alpha^3$  part of  $a_3$  from diagrams with vacuum polarization insertions are derived.

### I. INTRODUCTION

Some of the contributions from the 72 diagrams contributing to the  $\alpha^3$  part of the anomalous magnetic moment of the electron [ $a_e = \frac{1}{2}(g_e - 2)$ ] have already been calculated.<sup>1-4</sup> Recently the measurement of  $a_e$  has been performed by Wesley and Rich<sup>5</sup> with an accuracy of 6 ppm, so that a knowledge of the remaining contributions is urgently needed.

One of the main features of this kind of calculation is the amount of algebra involved. A great part of it can only be done reasonably by computer. In fact, in the above-mentioned calculations, computer techniques were broadly used. Two programs devoted to symbolic manipulations were mainly used: the REDUCE system of Hearn,<sup>6</sup> and

SCHOONSCHIP, a machine code program developed by Veltman.<sup>7</sup> In the method we are reporting, a slightly different method is used, and all the manipulations involved in the calculations are performed by a computer. The program written by one of us (J.C.) is intended to be general enough to calculate the contributions of all of the relevant diagrams. To do this, we had to develop a suitable method of renormalization and the appropriate calculational techniques. It appeared that the functional formalism framework<sup>8-10</sup> and the well-known Feynman method were suitable for our purpose.

The formulation of the renormalization theory in the framework of the functional formalism permits us to determine unambiguously the counterterms which have to be subtracted from a diagram to